Autocorrelations and intermediate-mass-fragment multiplicities in central heavy-ion collisions

W.J. Llope,[1,*] J.A. Conrad,[1,†] C.M. Mader,[1,‡] G. Peilert,[2] W. Bauer,[1]
D. Craig,[1] E. Gualtieri,[1] S. Hannuschke,[1] R.A. Lacey,[3] J. Lauret,[3] T. Li,[1]
A. Nadasen,[4] E. Norbeck,[6] R. Pak,[1] N.T.B. Stone,[1] A.M. Vander Molen,[1]
G.D. Westfall,[1] J. Yee,[1] and S.J. Yennello[5]

[1]*National Superconducting Cyclotron Laboratory, Michigan State University, East Lansing, Michigan 48824*
[2]*Lawrence Livermore National Laboratory, Livermore, California 94550*
[3]*Department of Chemistry, State University of New York–Stony Brook, Stony Brook, New York 11794*
[4]*Department of Physics, University of Michigan–Dearborn, Dearborn, Michigan 48128*
[5]*Cyclotron Institute, Texas A&M University, College Station, Texas 77843*
[6]*Department of Physics and Astronomy, University of Iowa, Iowa City, Iowa 52242*
(Received 18 April 1994; revised manuscript received 8 November 1994)

The average multiplicities of intermediate mass fragments (IMFs) for central heavy-ion collisions in the (nearly) symmetric entrance channels ^{20}Ne+^{27}Al, ^{40}Ar+^{45}Sc, ^{84}Kr+^{93}Nb, and ^{129}Xe+^{139}La, are systematically studied over a wide range of intermediate beam energies. Cuts on experimental variables commonly assumed to be correlated with the impact parameter are used to select the most central collisions. The results for six different centrality variables are compared, and the extent to which measurements of the multiplicities of IMFs in small impact parameter collisions are affected by the variable used to select the central events is discussed. General methods for locating such "autocorrelations" are described. The two centrality observables that are the least autocorrelated with the number of intermediate mass fragments are identified, and these variables are used to select the most central collisions. The entrance channel mass and beam energy dependence of the experimental IMF multiplicities are presented and compared to a variety of model predictions. The models picturing the disassembly as a sequential binary process always underpredict the experimental IMF multiplicities. A generally more accurate reproduction of these multiplicities is provided by several similar chemical equilibrium models commonly assumed to be the theoretical description of multifragmentation.

PACS number(s): 25.70.Pq

I. INTRODUCTION

Perhaps the most direct study of multifragment final states following intermediate energy heavy-ion collisions involves the experimental measurement of the average number of intermediate mass fragments (IMF's, for which $3 \leq Z \lesssim 20$) emitted in such reactions. A number of physical processes governing the disassembly of excited nuclei can result in the emission of such fragments [1, 2], and many software event generators embodying these processes are available. Most of these model codes fall into two general classes. One general class includes fundamentally "sequential binary" models, which describe the disassembly as a series of two-body decay steps, each involving (a)symmetric fission or statistical evaporation.

Another class is provided by a number of similar "multifragmentation" models, which assume chemical and thermal equilibrium has been obtained in an expanded spherical freeze-out volume of prescribed size. Generally, comparisons of the results obtained from models in these two classes imply that larger multiplicities of IMF's are obtained from the multifragmentation models, as compared to consistently run sequential binary calculations. Systematic experimental measurements of IMF emission from nuclear systems covering a wide range of mass and excitation energy are required, allowing the systematic confrontation of the various theoretical predictions with experimental results. Many experimental studies of IMF emission from systems formed over limited ranges of mass or excitation energy have already been published [3–27].

In this paper, the IMF emission from 27 different central heavy-ion reactions will be presented, including the entrance channels ^{20}Ne+^{27}Al, ^{40}Ar+^{45}Sc, ^{84}Kr+^{93}Nb, and ^{129}Xe+^{139}La. Each entrance channel was measured using the MSU 4π Array [28] at many beam energies ranging from 15 to 135 MeV/nucleon. The generation of the software events was done in both hybrid and dynamic approaches, and the events were filtered through a detailed software replica of the experimental apparatus. Comparisons of the average IMF multiplicities obtained

---

*Present address: T.W. Bonner Nuclear Laboratory, Herman Brown Hall, Rice University, Houston, TX 77251-1892. Electronic address: llope@physics.rice.edu

†Present address: Hughes STX, Goddard Space Flight Center, Code 921, Greenbelt, MD 20771.

‡Present address: Department of Physics, Hope College, Holland, MI 49423.

from the different models will be described. Also discussed is the extent to which the different model calculations reproduce the IMF multiplicities that were experimentally observed for the present systems of total mass from 47 to 268 and excitation energies from ~ 2 to ~ 25 MeV/nucleon.

Six experimental observables ("centrality variables") are assumed to be correlated with the impact parameter, and maximal values of each centrality variable are expected from the most central events. Cuts will be placed on these variables, allowing the experimental selection of the central nucleus-nucleus collisions in these data. It is noted, however, that the particular choice of the variable upon which a selection of central collisions is performed may affect the measurement of the average multiplicities of IMF's, due to constraints imposed on the reactions by charge or mass conservation laws.

The degree of "autocorrelation" between each of the six centrality variables and the average multiplicities of IMF's in these data must therefore be inferred. Such autocorrelations are an important source of bias for the study of any experimental observable following the selection of some impact parameter region. We assume that autocorrelations are reflected in the variances of the observable in different samples of events selected by cuts on many different centrality variables. The centrality cuts that artificially enhance or suppress the average multiplicities of IMF's in the most central events will be identified. Two-dimensional cuts will be placed on the two centrality variables that are the least autocorrelated with the multiplicities of IMF's for an internally unbiased measurement of this observable in the most central collisions. This will allow the comparison of the average IMF multiplicities obtained from the experimental and model generated events, and inferences concerning the validity of each model for the description of these multiplicities.

This paper is organized as follows. Section II describes the investigation of the autocorrelations between six different centrality variables and the observed multiplicities of IMF's. The centrality variables that are the least autocorrelated with the average multiplicities of IMF's, $\langle N_{\mathrm{IMF}} \rangle$, in small impact parameter collisions are defined. The entrance channel mass and beam energy dependence of $\langle N_{\mathrm{IMF}} \rangle$ in the central events selected using these nonautocorrelating variables are presented. The comparison of these experimental IMF multiplicities with those obtained from a number of filtered model codes is described in Sec. III. The summary and conclusions are presented in Sec. IV.

II. AUTOCORRELATIONS AND THE SELECTION OF CENTRAL COLLISIONS

In central heavy-ion reactions, highly excited nuclear systems can be formed that contain most of the nucleons in the entrance channel. The excitation energies in these systems are monotonic functions of the beam energy. Such events can be selected off line via software cuts on experimental variables that are correlated with the impact parameter. The variable upon which a centrality cut is made should be tightly correlated with the

impact parameter, and negligibly correlated with the experimental observable in all ways except that via the impact parameter.

A significant correlation between an experimental observable and the centrality variable (beyond that due to the impact parameter) can be caused by charge, mass, or momentum conservation laws. Such "autocorrelations" may artificially enhance or suppress the values of the experimental observable in the events selected by perfunctory centrality cuts. In this section, the degree of autocorrelation between six different centrality variables and the average multiplicities of IMF's in a comprehensive set of small impact parameter reactions will be investigated.

The experimental data were collected with the Michigan State University 4π Array [28] at the National Superconducting Cyclotron Laboratory (NSCL) using beams extracted from the K1200 cyclotron. Four symmetric entrance channels were systematically studied over a wide range of beam energies. The reactions include $^{20}\mathrm{Ne}+^{27}\mathrm{Al}$ at 55, 75, 95, 105, 115, 125, and 135 MeV/nucleon, $^{40}\mathrm{Ar}+^{45}\mathrm{Sc}$ at 15, 25, 35, 45, 65, 75, 85, 105, and 115 MeV/nucleon, $^{84}\mathrm{Kr}+^{93}\mathrm{Nb}$ at 35, 45, 55, 65, and 75 MeV/nucleon, and $^{129}\mathrm{Xe}+^{139}\mathrm{La}$ at 25, 35, 45, 50, 55, and 60 MeV/nucleon. Detailed descriptions of the apparatus and the data collection can be found in Refs. [28, 29].

There is an intrinsic width to experimental observables in perfectly central collisions that is caused by the stochastic nature of the evolution of the excited nuclear systems formed in these collisions. Additional experimental contributions to this width result from any dependence of the experimental acceptance on the orientation of these excited systems in the laboratory, and from any inefficiencies in the selection of the most central collisions. These experimental contributions can be understood via the study of the effect that a software replica of the experimental apparatus has on events generated by model codes at specific impact parameters (see Sec. III). In principle, the intrinsic width carries important physical information concerning fluctuations during the reactions. The measured width can, after the treatment of the experimental contributions, be defined as the intrinsic width, unless there are non-negligible autocorrelations between the observable O and the experimental variable used to select the central events.

It is assumed that the variance $\sigma_O^2 = \langle O^2 \rangle - \langle O \rangle^2$ of an observable O in a sample of selected events is suppressed if a significant autocorrelation exists, and is equal to the intrinsic variance or width (modified by experimental considerations) otherwise. The importance of such autocorrelations during the use of a particular centrality variable can thus be inferred by the comparison of the variance of the observable following the selection of central events using many different centrality variables. The cut(s) leading to the largest variances σ_O^2 in the selected events are assumed to be the least autocorrelated with O. Two classes of autocorrelations between a centrality cut and an experimental observable can be defined based on the effects that such autocorrelations have on the normalized variance $\sigma_O^2 / \langle O \rangle$ in the selected events. Centrality cuts which result in a suppressed variance and

a suppressed (enhanced) normalized variance will be referred to as positive (negative) autocorrelators, as they artificially enhance (suppress) $\langle O \rangle$.

The following variables are assumed to be correlated with the impact parameter: (i) the number of charged particles (N_{chgd}) detected in each event, (ii) the total charge detected in a software gate centered at midrapidity (Z_{MR}), (iii) the total transverse kinetic energy (E_T), (iv) the number of detected hydrogen isotopes (N_H), (v) the total detected charge (Z_{det}), and (vi) the total charge of hydrogen and helium isotopes particles (Z_{LCP}). The variables Z_{MR} and E_T are defined as in Ref. [30]. Separate samples of events are formed by placing thresholds on the impact-parameter-inclusive spectra of each of these variables which allow the most central $\sim$10% of the events. For all of the centrality variables that are integer quantities, i.e., all but E_T, it is not always possible to locate a threshold such that exactly 10% of the minimum bias events are selected. The threshold was thus defined for each centrality variable and reaction as the lowest bin for which $\leq$10% of the impact-parameter-inclusive events are in or above this bin. According to approximate geometrical arguments, thresholds allowing 10% of the impact-parameter-inclusive events allow average impact parameters $\langle b \rangle \sim 0.31 b_{max}$. The quantity b_{max} is the largest impact parameter satisfying the minimum bias trigger used to collect these data, which required two or more charged particle hits in the MSU 4π Array. The quantity b_{max} has typically been assumed to equal $[R_P + R_T]$, where R_P (R_T) is the radius of the projectile (target) nucleus; this assumption is tested below.

In Figs. 1 and 2, the means (upper frames), variances

FIG. 2.   The same as Fig. 1, except for the ^{84}Kr$+^{93}$Nb and ^{129}Xe$+^{139}$La entrance channels.
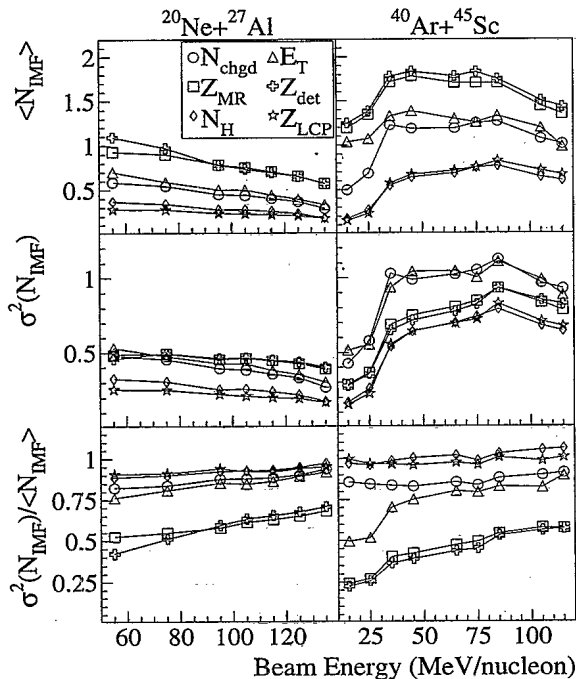

FIG. 1.   The means, variances, and normalized variances of the IMF multiplicities versus the beam energy in the six separate samples of small impact parameter events for the ^{20}Ne$+^{27}$Al and ^{40}Ar$+^{45}$Sc entrance channels.

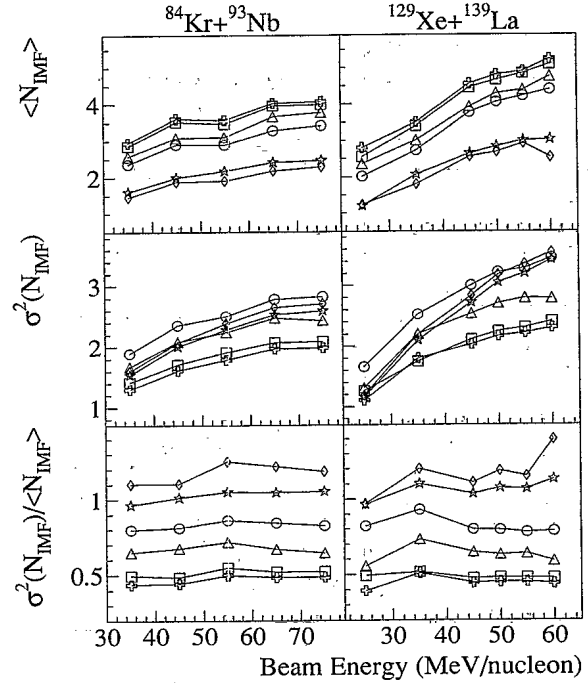(middle frames), and normalized variances (lower frames) of the N_{IMF} distributions are presented versus the beam energy in the six samples of selected small impact parameter events. The ^{20}Ne$+^{27}$Al and ^{40}Ar$+^{45}$Sc entrance channels are shown in Fig. 1, while the ^{84}Kr$+^{93}$Nb and ^{129}Xe$+^{139}$La reactions are shown in Fig. 2. The statistical errors in these figures are smaller than the size of the points, while the systematic errors are discussed in Sec. III.

For all four entrance channels, the beam energy dependence of the IMF multiplicity observables is generally not affected by the particular choice of the variable used to select the small impact parameter events. In the ^{20}Ne$+^{27}$Al reactions $(E_{proj} \geq 55$ MeV/nucleon), the values of $\langle N_{IMF} \rangle$ decrease with increasing beam energies. In the ^{40}Ar$+^{45}$Sc reactions, the experimental values of $\langle N_{IMF} \rangle$ increase with increasing beam energies up to about 35 MeV/nucleon, and then fall off slowly for larger beam energies. For both of the heavier systems, ^{84}Kr$+^{93}$Nb $(E_{proj} \leq 75$ MeV/nucleon) and ^{129}Xe$+^{139}$La $(E_{proj} \leq 60$ MeV/nucleon), the values of $\langle N_{IMF} \rangle$ increase with increasing beam energies.

In Figs. 1 and 2, the IMF multiplicity observables in the events selected by the six different centrality cuts generally form three distinct groups independent of the beam energy. Centrality cuts on the variables Z_{MR} and Z_{det} result in N_{IMF} distributions with relatively small variances and small normalized variances, while cuts on the variables N_H and Z_{LCP} result in relatively small variances and relatively large normalized variances. The events selected by the cuts on the variables N_{chgd} and E_T have the relatively largest variances and intermediate normalized variances. Some exceptions to these trends in $\sigma^2(N_{IMF})$ are noted. At the highest beam energies in the ^{20}Ne$+^{27}$Al

entrance channel, the variances following the Z_{MR} and Z_{det} cuts exceed those following the N_{chgd} and E_T cuts. In the two heavier systems (Fig. 2), the variances from the N_H and Z_{LCP} cuts are similar to those from the N_{chgd} and E_T cuts (and relatively large). However, for all of the reactions, the normalized variances are always ordered in the same way.

The formation of these groups is generally independent of the beam energy and the entrance channel mass, which implies that the grouping is the consequence of an internal effect rather than a physical one. The formation of these groups is a reflection of autocorrelations between some of these centrality variables and N_{IMF}. The centrality variables N_H and Z_{LCP} apparently suppress $\langle N_{IMF} \rangle$ (and σ^2) and are thus defined to be negative autocorrelators, while the variables Z_{MR} and Z_{det} artificially enhance $\langle N_{IMF} \rangle$ and are labeled positive autocorrelators. Given the dramatic distortions to IMF multiplicity observables seen in Figs. 1 and 2 that result from centrality cuts on variables that autocorrelate with N_{IMF}, the only study of these observables in the central collisions in these data that is free from such distortions must involve centrality cuts on N_{chgd} and/or E_T. Figures 1 and 2 imply that the negative autocorrelation between the light-particle multiplicity variables and N_{IMF} is somewhat stronger than the positive autocorrelation between N_{IMF} and the variables Z_{MR} and Z_{det}.

To limit the selection of larger impact parameter events with significant topological fluctuations, a two-dimensional cut [30] is placed on the centrality variables N_{chgd} and E_T for all of the systems and beam energies. Only the events that fall above the thresholds located as described above (each allowing $\lesssim 10\%$ of the events) for both of these variables are selected. This results in the selection of ~ 4–7% of the events, which have average impact parameters $\langle b \rangle \sim 0.20 b_{max}$–$0.26 b_{max}$ geometrically.

Simulations were performed using the event generator FREESCO [31] and a complete description of the acceptance, as described in Sec. III, to test the assumption that $b_{max} = [R_P + R_T]$ in the present experimental data. The dependence of $\langle N_{IMF}^{sim} \rangle$ on the impact parameter, $0 \le b_{sim} \le [R_P + R_T]$, was extracted from the filtered events generated for a number of representative reactions. A "reduced" impact parameter $\hat{b}$ for each experimental event was constructed using the geometrical prescription described in Ref. [32]. These impact parameter scales were constructed using the minimum bias spectra of N_{chgd} and E_T, separately. The N_{IMF} versus $\hat{b}$ distributions obtained from these two centrality variables are similar. We then compared the experimental dependence of $\langle N_{IMF} \rangle$ on $\hat{b}$ with the dependence of $\langle N_{IMF}^{sim} \rangle$ on b_{sim} obtained from the filtered simulations. These two dependences agree if one assumes that $b_{max} \sim (0.65 \pm 0.10)[R_P + R_T]$ for the ^{20}Ne+^{27}Al reactions, and $b_{max} \sim (0.91 \pm 0.06)[R_P + R_T]$ for the ^{129}Xe+^{139}La reactions. This implies that the present selection of ~ 4–7% of the minimum bias events is somewhat more central than predicted simply from the geometrical prescription ($\langle b \rangle \sim 0.20 b_{max}$–$0.26 b_{max}$) and the assumption that $b_{max} = [R_P + R_T]$.

The mean multiplicities of IMF's in the selected events

are shown for all of the entrance channels and beam energies in Fig. 3 as the solid squares. The average IMF multiplicities in the events selected by the two one-dimensional cuts on N_{chgd} (open circles) and E_T (open triangles) are also shown. The events selected by the two-dimensional cut exhibit larger values of $\langle N_{IMF} \rangle$ as compared to those following either of the one-dimensional cuts. For increasing beam energies, the values of $\langle N_{IMF} \rangle$ decrease in the central ^{20}Ne+^{27}Al reactions ($E_{proj} \ge 55$ MeV/nucleon), rise and then fall in the central ^{40}Ar+^{45}Sc reactions, and increase in the central ^{84}Kr+^{93}Nb ($E_{proj} \le 75$ MeV/nucleon) and ^{129}Xe+^{139}La reactions ($E_{proj} \le 60$ MeV/nucleon). The average IMF multiplicities range from ~ 0.4 for the highest energy ^{20}Ne+^{27}Al reactions to ~ 5.5 for the highest energy ^{129}Xe+^{139}La reactions

The variances $\sigma^2(N_{IMF})$ in these same samples of small impact parameter events are shown in Fig. 4. The variances from the two-dimensional $\sim 10\%$ cuts (solid squares) are larger than the variances from the two one-dimensional cuts (open circles and triangles) in the ^{20}Ne+^{27}Al and ^{40}Ar+^{45}Sc reactions, and they are similar to or between the values from the two one-dimensional cuts in the ^{84}Kr+^{93}Nb and ^{129}Xe+^{139}La reactions. Also shown in this figure are the N_{IMF} variances from stricter two-dimensional $\sim 2\%$ cuts on N_{chgd} and E_T (solid triangles). It is important to note that the N_{IMF} variances from these stricter two-dimensional $\sim 2\%$ cuts are always larger than those from the two-dimensional $\sim 10\%$ cuts (solid squares). This corroborates the statement that the variables N_{chgd} and E_T do not autocorrelate with
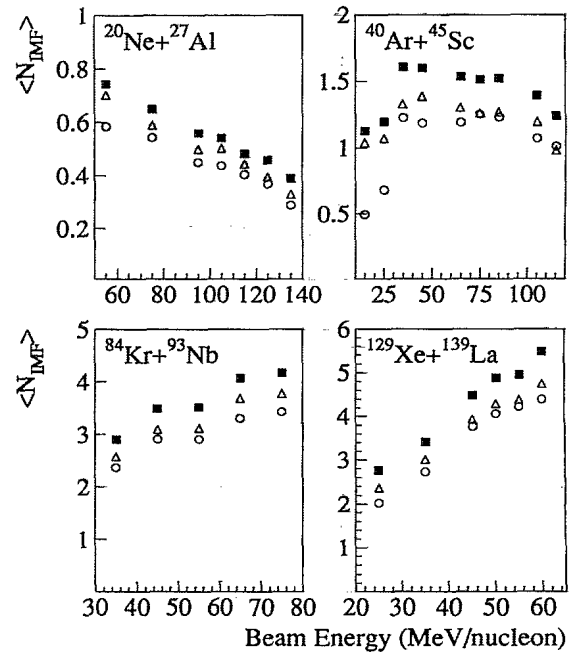
FIG. 3. The average number of IMF's versus the beam energy for three samples of small impact parameter events. Shown are the results following the two-dimensional $\sim 10\%$ cuts on N_{chgd} and E_T (solid squares), and following the two one-dimensional $\sim 10\%$ cuts on N_{chgd} (open circles) and E_T (open triangles).
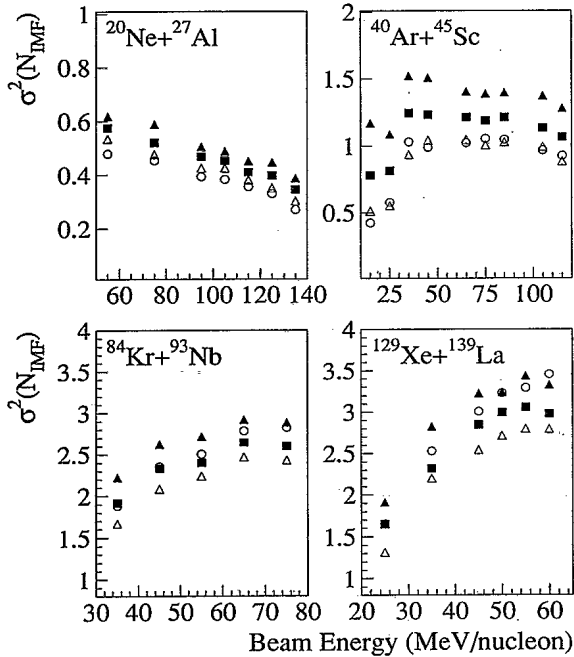
FIG. 4. The same as Fig. 3, except for the N_{IMF} variances in same samples of small impact parameter events. Also shown are these variances following two-dimensional ~2% cuts on N_{chgd} and E_T (solid triangles).

N_{IMF} in these data, as stricter cuts must magnify the importance of the conservation law that drives the autocorrelation.

The average multiplicities of IMFs are depicted versus the total charged particle multiplicity in Fig. 5. For all of the available entrance channels and beam energies, the largest average multiplicities of IMFs are found in the
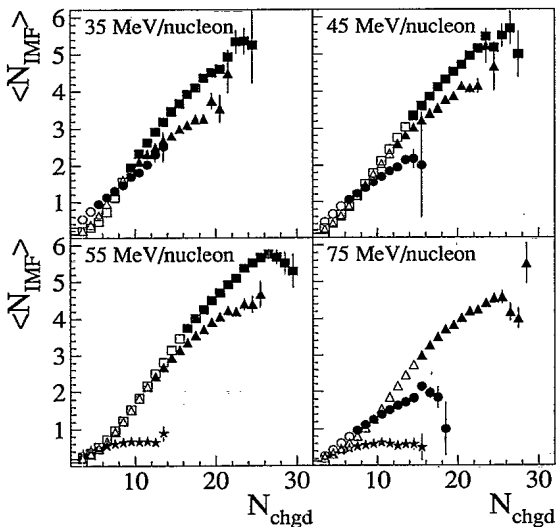

FIG. 5. The average number of IMF's versus the total charged particle multiplicity for $^{20}Ne+^{27}Al$ (stars), $^{40}Ar+^{45}Sc$ (circles), $^{84}Kr+^{93}Nb$ (triangles), and $^{129}Xe+^{139}La$ (squares) reactions at four representative beam energies. The values for events above the ~10% most central thresholds on N_{chgd} are depicted as the solid points.

events with the largest total charged particle multiplicities. In this figure, the solid points for each system and beam energy are those above the ~10% cuts on N_{chgd} alone described above. A roughly universal dependence of $\langle N_{IMF} \rangle$ on N_{chgd} is noted for the more peripheral collisions (open points). A similar observation was made in, e.g., Ref. [25].

A number of different model calculations were used to predict the values of $\langle N_{IMF} \rangle$ that would occur in a sequential binary or multifragmentation scenario for the disassembly. These calculations were also used to evaluate the accuracy by which models attempting to describe these scenarios can reproduce the experimentally measured values of $\langle N_{IMF} \rangle$. All of the inefficiencies in the apparatus were included in the software. These simulations and comparisons to the data are described in the next section.

III. MODEL PREDICTIONS

Many different physical mechanisms that may govern the disassembly of excited nuclei can lead to the emission of intermediate mass fragments [1, 2]. In this section, we describe the results obtained from models that embody assumptions from a variety of theoretical approaches for describing central intermediate energy heavy-ion collisions. The purpose of these calculations is twofold. First, the different calculations are performed as consistently as possible, so that the average IMF multiplicities from the different models can be directly compared. Second, under the assumption that the chosen input parameters to the different calculations are realistic, the average IMF multiplicities from the models can be directly compared to the experimentally measured values described in the previous section.

A. The event generation

The event generation was performed in both dynamic and hybrid approaches. The "afterburners" used in the hybrid event generation were the BERLIN [33] and COPENHAGEN [34] multifragmentation codes, as well as the sequential binary code GEMINI [35]. The BERLIN and COPENHAGEN codes are similar in philosophy, and assume that the system comes to thermal and chemical equilibrium within an expanded volume that is spherical and of prescribed radius. The various fragmentation channels occur with probabilities obtained from the channels' entropy, which is obtained using a finite temperature liquid-drop model. The code GEMINI pictures the disassembly as a sequence of binary fissions, using Bohr-Wheeler fission widths and conditional barriers from a shape adjusted two-spheroid finite range calculation, followed by evaporation according to a Hauser-Feshbach description.

All of these calculations were run with the default parameters with the exception of the charge, mass, and excitation energy in the composite system, which was extracted from Boltzmann-Uehling-Uehlenbeck (BUU) calculations [36] in the same manner as described in Ref. [25]. These calculations describe the evolution of the one-

body phase space distribution following the Boltzmann equation, including approximately Pauli-blocked scattering, via ensemble averaging. A soft equation of state was assumed, and the calculations were terminated when the radial density profile of the composite system most closely resembled that of a ground state nucleus [37]. The excitation energy of the excited system at rest in the center of momentum (CM) frame is then calculated as the total energy of this system minus a liquid-drop energy for a ground state nucleus with the same charge and mass. The calculations were performed at an impact parameter of $b = 0.2[R_P + R_T]$.

The excitation energies predicted by the BUU calculations for the selected events in each reaction are shown in Fig. 6. A recent analysis [38] has noted differences in the IMF multiplicities obtained when an afterburner code is supplied with a single average excitation energy or excitation energies separately calculated for each event. However, given the large number of different reactions and afterburner model codes studied here, a dynamic calculation of the afterburner input parameters for each generated event is computationally prohibitive. The mass and charge of the composite predicted by the BUU calculations is generally ~90% of the total entrance channel mass and charge. In the present BUU hybrid event generation, the remaining particles are thermally emitted from projectile and targetlike sources, using reasonable assumptions for the velocities, temperatures, and emitted charge distributions of these sources for each reaction.

The BERLIN and GEMINI codes also require a cutoff angular momentum. For the BUU + BERLIN calculations, the values used were $36\hbar$, $62\hbar$, $80\hbar$, and $70\hbar$ for the central ^{20}Ne+^{27}Al, ^{40}Ar+^{45}Sc, ^{84}Kr+^{93}Nb, and ^{129}Xe+^{139}La reactions, respectively. The angular momenta of the excited systems in the selected experimental events may very well exceed the values assumed above, presumably leading to decays involving a fast fission.
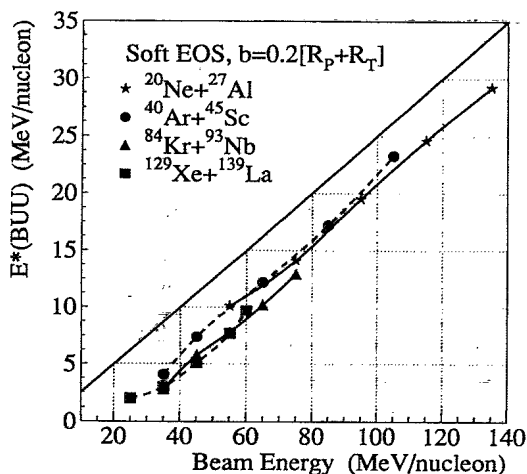

FIG. 6. The excitation energies extracted from the BUU calculations for the ^{20}Ne+^{27}Al (stars), ^{40}Ar+^{45}Sc (circles), ^{84}Kr+^{93}Nb (triangles), and ^{129}Xe+^{139}La (squares) reactions, assuming an average impact parameter geometrically consistent with the present central event selection and a soft equation of state.

The BUU + GEMINI calculations were therefore also performed using cutoff angular momenta both well above and below the values listed above.

Complete events from a hybrid model involving a quantum molecular dynamics (QMD) [39] initial stage and COPENHAGEN disassembly were also produced for ^{36}Ar+^{45}Sc reactions for impact parameters $b \leq 4$ fm. The QMD calculations describe the evolution of a system of Gaussian wave packets (nucleons) that move under the influence of mutual two- and three-body forces and scatter in approximate respect of the Pauli principle. Although hybrid in the sense that the reaction is described in two steps, the QMD + COPENHAGEN calculations are dynamic in the sense that the impact parameter for each calculated event is known. Another model with this feature is the code FREESCO [31], which does not require a separate BUU or QMD description of the initial stage of the reaction. This model divides the colliding nuclei into two spectator sources and a participant source, which share energy and angular momenta, according to the impact parameter. The decay of these sources is described by a microcanonical calculation similar in philosophy to those in the BERLIN and COPENHAGEN models, including a simplified description of the evaporation.

A software reproduction of the experimental apparatus is used to filter the events obtained in all of the approaches listed above. This code contains a detailed treatment of the geometry of the device including all inactive regions, the run-dependent particle kinetic energy thresholds for all measurable particles, the particle kinetic energy loss in the target and associated support assembly, and multiple particle hits in individual detector elements. The calculation of the result of a multiple hit involves the same particle charge and energy templates used to calibrate all of the raw experimental data. Following the passage through the filter code, the generated events appear as they would experimentally, up to a conservatively assumed systematic uncertainty of ~30% in the values of $\langle N_{\text{IMF}} \rangle$ from the filtered simulations.

The multiplicities of IMF's can also be calculated using model codes which do not generate samples of complete events. Examples of these are the statistical evaporation code STAT, described in Ref. [40], and the quantum statistical model [41]. The model of Ref. [40] follows the ensemble averaged evolution of a system that statistically emits particles in a sequence of two-body decay steps. This model thus provides a description of sequential binary disassembly that is alternative to the (fission-evaporation) GEMINI code. The Fermi energy used as input in this model was 25 MeV for the central ^{20}Ne+^{27}Al and ^{40}Ar+^{45}Sc reactions, and 30 MeV for the central ^{84}Kr+^{93}Nb and ^{129}Xe+^{139}La reactions [42]. However, as complete events are not provided by this code, the experimental inefficiencies for the measurement of N_{IMF} can only be imposed approximately. This is done by extracting the average efficiency for detecting IMFs from each of the filtered event-generating models listed above for all entrance channels and beam energies. These efficiencies are generally between 50% and 80%, depending on the reaction and the approach used to generate the complete events. For each reaction separately, the

minimum and maximum IMF measurement efficiencies obtained from the different model calculations are multiplied by the IMF multiplicities obtained from the statistical evaporation code. This defines a range of IMF multiplicities for each reaction presumed to contain the predictions of the statistical evaporation code including the effects of the experimental inefficiencies.

B. Comparisons to the data

Many previously published studies of IMF production included comparisons of experimental results to those obtained from model calculations. These employed dynamical codes alone (using the models BUU [16], BNV [24], QMD [21, 27], and QPD [14, 27]), afterburner codes alone (using the models BERLIN [19, 20], COPENHAGEN [19, 26], GEMINI [8, 17, 19, 20, 26], STAT [17], and EES [14, 17]), as well as hybrid calculations (using the models BNV+GEMINI [24], BUU+GEMINI [25], BUU+STAT [25], QMD+COPENHAGEN [21, 27], BUU+EES [25], and QPD+EES [27]).[1] Systematic experimental measurements versus the beam energy [4, 8, 13, 14, 21, 27], the target nucleus [3, 4, 6, 8, 9, 15, 16, 19, 24, 25], and/or the impact parameter [15, 16, 19, 23, 26] have been used to explore the excitation energy and system mass dependence of IMF emission. In this section, we describe comparisons of all of the models described in Sec. III A with a data set that is systematic in both the entrance channel mass and beam energy for central heavy-ion collisions in symmetric entrance channels.

The average IMF multiplicities in the central ^{20}Ne+^{27}Al, ^{40}Ar+^{45}Sc, ^{84}Kr+^{93}Nb, and ^{129}Xe+^{139}La reactions are shown in Figs. 7–10, respectively. The experimental values from the two-dimensional ~10% central cut (on N_{chgd} and E_T) are shown by the solid points, while the values from the two one-dimensional ~10% cuts (on N_{chgd} and E_T, separately) are given by the open points.

The lines in Figs. 7–10 depict the results from the various model calculations. The lines in the upper frames are the values of $\langle N_{IMF} \rangle$ predicted by the filtered BUU+ BERLIN (solid) and BUU+ COPENHAGEN (dashed) calculations. In Fig. 8 only, the upper frame also includes the predictions of the filtered QMD+COPENHAGEN calculations, which were run under the same assumptions used to generate the BUU+BERLIN and BUU+COPENHAGEN events. The lines in the middle frames depict the predictions of the filtered FREESCO code, which was run for maximum impact parameters of $0.01(R_P + R_T)$ (solid), $0.20(R_P + R_T)$ (dashed), and $0.40(R_P + R_T)$ (dot-dashed). The lower frames include the predictions of the filtered BUU+GEMINI calculations, which were performed for maximum angular momenta of $10\hbar$ (solid), $70\hbar$ (dashed), and $200\hbar$ (dot-dashed).

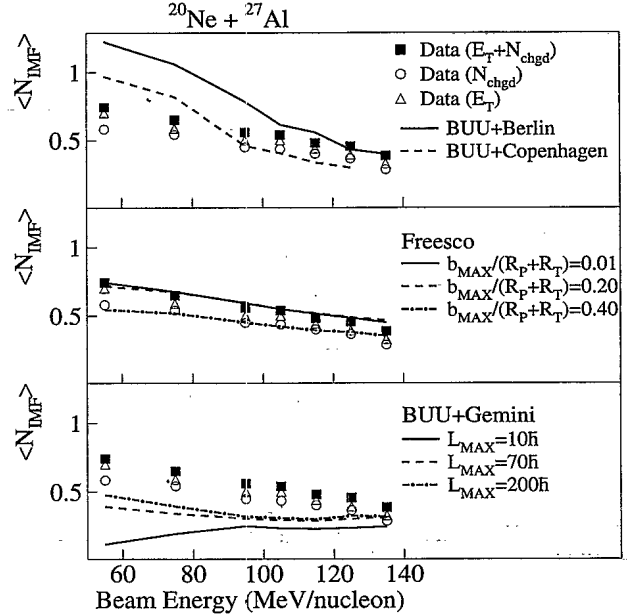The experimental IMF multiplicities in the cen-

FIG. 7. The average IMF multiplicities versus the beam energy in the central ^{20}Ne+^{27}Al reactions. The points are the experimental results for the events selected by the two-dimensional ~10% cuts on N_{chgd} and E_T (solid squares), the one-dimensional ~10% N_{chgd} cuts (open circles), and the one-dimensional ~10% E_T cuts (open triangles). The lines depict the results from the various filtered model calculations (see text).

tral ^{20}Ne+^{27}Al reactions (Fig. 7) at beam energies near and above 100 MeV/nucleon agree with the BUU+BERLIN, BUU+COPENHAGEN, and FREESCO calculations. For lower beam energies in this system, however, the BUU+BERLIN and BUU+COPENHAGEN calculations overestimate the experimental values. The cal-
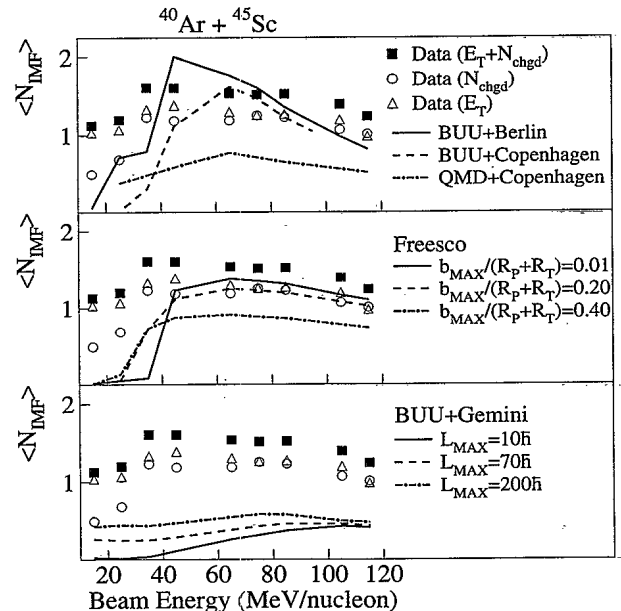

FIG. 8. The same as Fig. 7, except for the central ^{40}Ar+^{45}Sc reactions.

[1]BNV corresponds to Boltzmann-Nordhiem-Vlasov calculations [24], EES is the expanding evaporating source model [43], and QPD is the quasiparticle dynamics model [44].
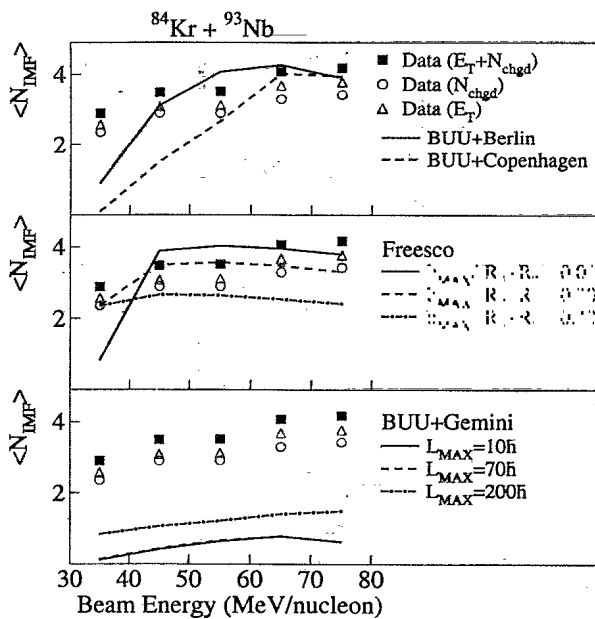
FIG. 9. The same as Fig. 7, except for the central ^{84}Kr+^{93}Nb reactions.

culated IMF multiplicities increase slowly with decreasing maximum impact parameters in the filtered FREESCO calculations. The IMF multiplicities obtained from the filtered BUU+GEMINI events increase with increases in the maximum angular momentum allowed in the calculation. However, even for maximum angular momenta well in excess of that which can be supported by the systems expected to be formed in the central ^{20}Ne+^{27}Al collisions, the BUU+GEMINI IMF multiplicities underpredict the experimental values.
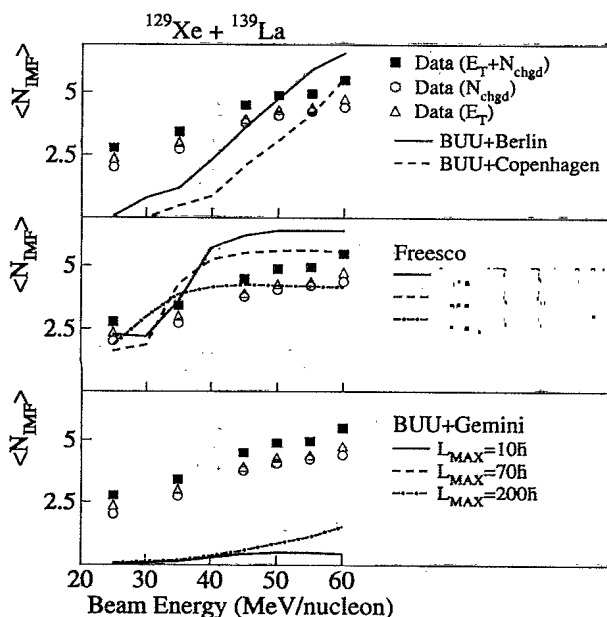
The filtered BUU+BERLIN and BUU+COPENHAGEN

FIG. 10. The same as Fig. 7, except for the central ^{129}Xe+^{139}La reactions.

calculations predict (Fig. 8) a sharp rise in the IMF multiplicities for the central ^{40}Ar+^{45}Sc reactions near beam energies of 40 MeV/nucleon. The experimental IMF multiplicities for these reactions exhibit such a rise for beam energies somewhere between 25 and 35 MeV/nucleon. These two approaches significantly underestimate the experimental IMF multiplicities below 35 MeV/nucleon, and reasonably reproduce the experimental values for larger beam energies.

The QMD+COPENHAGEN calculations predict about a factor of 2 fewer IMF's than observed experimentally for all beam energies. These QMD+COPENHAGEN predictions are quite insensitive to the stiffness of the equation of state used in the QMD phase, or the radius of the critical freeze-out volume assumed in the subsequent COPENHAGEN calculation, for all of the central ^{40}Ar+^{45}Sc reactions. One possible cause of the different IMF multiplicities obtained from the BUU+COPENHAGEN and the QMD+COPENHAGEN calculations involves the differences in the treatment of Pauli blocking in the two dynamical codes. Indeed, Donangelo *et al.* recently questioned the validity of this treatment in molecular dynamics codes [45]. These authors claim an overprediction of the nuclear heat capacity in molecular dynamics codes hinders the production of IMF's in such calculations, which is consistent with the results shown in Fig. 8.

The filtered FREESCO calculations predict a sharp rise in the IMF multiplicities near 35–45 MeV/nucleon, depending on the impact parameter region allowed in the calculation. These calculations generally reproduce the experimental results at beam energies above $\sim$45 MeV/nucleon if $b_{max} \lesssim 0.2(R_P + R_T)$, and again lead to significant underestimates at lower beam energies. The BUU+GEMINI calculations significantly underestimate the experimental IMF multiplicities for all three values of the maximum angular momenta allowed in these calculations and for all beam energies.

The conclusions drawn for the central ^{84}Kr+^{93}Nb (Fig. 9) and ^{129}Xe+^{139}La (Fig. 10) reactions are generally similar to those drawn from the central ^{40}Ar+^{45}Sc reactions. The BUU+BERLIN and BUU+COPENHAGEN calculations underestimate the experimental IMF multiplicities at the lowest available beam energies, and provide a better reproduction of the experimental values at larger beam energies. The filtered FREESCO calculations give a reasonable description of the IMF multiplicities for all of the available beam energies in these entrance channels. The BUU+GEMINI calculations again lead to underestimates for all beam energies and maximum angular momenta allowed in the calculation.

The comparison of the experimental IMF multiplicities and those from the statistical evaporation code of Ref. [40], following the approximate treatment of the experimental inefficiencies, is shown in Fig. 11. For all of the reactions studied in this analysis, these calculations significantly underpredict the observed IMF multiplicities. This underprediction is similar to that from the filtered BUU+GEMINI calculations. A similar inability of this statistical evaporation code to reproduce experimental IMF multiplicities was described in Ref. [25].

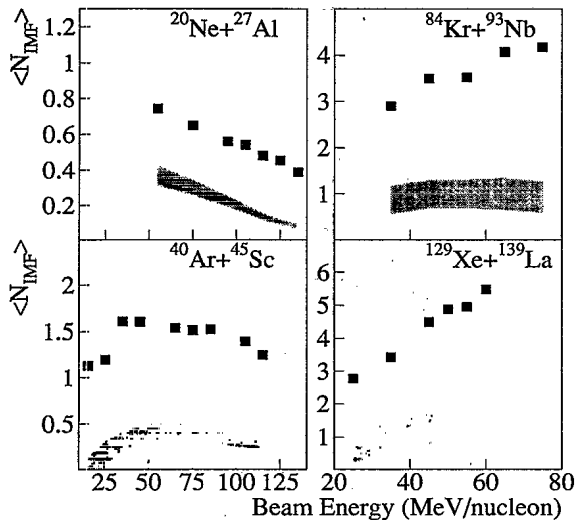It is interesting to note that the code FREESCO is ap-

FIG. 11. The average IMF multiplicities versus the beam energy for the small impact parameter events selected by the two-dimensional $\sim$10% cuts on N_{chgd} and E_T (solid squares) for all four entrance channels. The shaded regions depict the average IMF multiplicities obtained from the statistical evaporation model of Ref. [40], after an approximate treatment of the experimental acceptance (see text).

parently as capable of reproducing the experimental IMF multiplicities as the more complicated and CPU-intensive BUU+BERLIN and BUU+COPENHAGEN hybrid calculations. This reproduction of the experimental IMF multiplicities by the filtered FREESCO calculations is, however, somewhat accidental, as this code generally overpredicts the IMF kinetic temperatures by about 20–30 %. This leads to underestimates of IMF losses due to experimental kinetic energy thresholds, and hence overestimates of the average IMF multiplicities by approximately 0.2–0.4 IMFs.

IV. SUMMARY AND CONCLUSIONS

This analysis has investigated the average multiplicities of intermediate mass fragments emitted following central heavy-ion reactions in four near symmetric entrance channels, each at many intermediate beam energies. The average IMF multiplicities were shown to be significantly affected by possible autocorrelations with the variables upon which the impact parameter of each event was inferred. Six different centrality variables were compared, and those variables that are not autocorrelated with the IMF multiplicities for small impact parameter collisions were identified. These variables were the total charged particle multiplicity and the total transverse kinetic energy. Experimental observables other than the IMF multiplicities were not studied in this paper, but general methods allowing the identification of autocorrelating centrality cuts for any experimental observable were described.

Predictions for the average multiplicities of IMFs in small impact parameter collisions were obtained from a variety of theoretical model codes. These predictions were filtered through a detailed software replica of the experimental apparatus. The average IMF multiplicities obtained from the two sequential binary models were always less than those obtained from the multifragmentation models. The experimental results were generally more accurately described by the multifragmentation models, with notable exceptions from some of these models for beam energies near and below $\sim$35 MeV/nucleon.

[1] E. Saraud, Ch. Grégoire, and B. Tamain, Prog. Nucl. Part. Sci. **23**, 357 (1989), and references therein; D.H.E. Gross, Rep. Prog. Phys. **53**, 605 (1990), and references therein; L.G. Moretto and G.J. Wozniak, Annu. Rev. Nucl. Part. Sci. **43**, 379 (1993), and references therein; H. Fuchs and K. Möhring, Rep. Prog. Phys. **57**, 231 (1994), and references therein.

[2] *Proceedings of the Third International Conference on Nucleus-Nucleus Collisions*, edited by C. Détraz, C. Estéve, C. Grégoire, D. Guerreau, and B. Tamain [Nucl. Phys. **A488** (1988)]; *Proceedings of the International Workshop on Nuclear Dynamics at Medium and High Energies*, edited by W. Cassing and U. Mosel [*ibid.* **A495** (1,2) (1989)]; *Proceedings of the International Workshop on Nuclear Dynamics*, edited by P.F. Bortignon, M. Di Toro, S. Fantoni, I. Iori, and S. Stringari [*ibid.* **A519**, (1,2) (1990)]; *Proceedings of the Fourth International Conference on Nucleus-Nucleus Collisions*, edited by H. Toki, I. Tanihata, and H. Kamitsubo [*ibid.* **A538** (1992)]; *Proceedings of the International Workshop on Dynamical Fluctuations and Correlations in Nuclear Col-*

lisions, edited by M. Bex, B. Borderie, M. Ploszajczak, J. Richert, P. Schuck, and E. Saraud [*ibid.* **A545**, (1,2) (1992)].

[3] D. Pelte, U. Winkler, J. Pochodzalla, M. Bühler, A. Gorks, and B. Weissmann, Nucl. Phys. **A438**, 532 (1985); D. Pelte, U. Winkler, M. Bühler, B. Weissmann, A. Gobbi, K.D. Hildenbrand, H. Stelzer, and R. Novotny, Phys. Rev. C **34**, 1673 (1986); D. Pelte, U. Winkler, M. Gnirs, A. Gobbi, K.D. Hildenbrand, and R. Novotny, *ibid.* **39**, 553 (1989).

[4] G. Klotz-Engmann, H. Oeschler, E. Kankeleit, Y. Cassagnou, M. Conjeaud, R. Dayras, S. Harar, M. Mostefai, R. Legrain, E.C. Pollacco, and C. Volant, Phys. Lett. B **187**, 245 (1987).

[5] D.R. Bowman, W.L. Kehoe, R.J. Charity, M.A. McMahan, A. Moroni, A. Bracco, S. Bradley, I. Iori, R.J. MacDonald, A.C. Mignerey, L.G. Moretto, M.N. Namboodiri, and G.J. Wozniak, Phys. Lett. B **189**, 282 (1987).

[6] R. Trockel, U. Lynen, J. Pochodzalla, W. Trautmann, N. Brummund, E. Eckert, R. Glasow, K.D. Hildenbrand, K.H. Kampert, W.F.J. Müller, D. Pelte, H.J. Rabe, H.

Sann, R. Santo, H. Stelzer, and R. Wada, Phys. Rev. Lett. **59**, 2844 (1987).

[7] A.S. Botvina, A.S. Iljinov, and I.N. Mishustin, Phys. Lett. B **205**, 421 (1988).

[8] R. Trockel, K.D. Hildenbrand, U. Lynen, W.F.J. Müller, H.J. Rabe, H. Sann, H. Stelzer, W. Trautmann, R. Wada, E. Eckert, P. Kruetz, A. Kühmichel, J. Pochodzalla, and D. Pelte, Phys. Rev. C **39**, 729 (1989).

[9] J. Pochodzalla, R.J. Charity, U. Lynen, H. Sann, W. Trautmann, and R. Trockel, Phys. Rev. C **40**, 2918 (1989).

[10] R. Bougault, J. Colin, F. Delaunay, A. Genoux-Lebain, A. Hajfani, C. le Brun, J.F. Lecolley, M. Louvel, and J.C. Steckmeyer, Phys. Lett. B **232**, 291 (1989).

[11] H.Y. Han, K.X. Jing, E. Plagnol, D.R. Bowman, R.J. Charity, L. Vinet, G.J. Wozniak, and L.G. Moretto, Nucl. Phys. **A492**, 138 (1989).

[12] J. Boger, S. Kox, G. Auger, J.M. Alexander, A. Narayanan, M.A. MacMahan, D.J. Moses, M. Kaplan, and G.P. Gilfoyle, Phys. Rev. C **41**, R801 (1990).

[13] U. Milkau, E. Berdermann, B. Berthier, P. Bouissou, C. Cerruti, A. Demeyer, E.-M. Eckert, D. Guinet, K.D. Hildenbrand, J. Hubele, G. Imme, P. Kreutz, A. Kühmichel, G.J. Kunde, S. Leray, P. Lhénoret, R. Lucas, U. Lynen, C. Mazur, W.F.J. Müller, C. Ngô, C.H. Pickenburg, J. Pochodzalla, H.J. Rabe, G. Raciti, M. Ribrag, H. Sann, H. Stelzer, E. Tomasi, W. Trautmann, R. Trockel, and R. Wada, Phys. Rev. C **44**, R1242 (1991).

[14] R.T. de Souza, L. Phair, D.R. Bowman, N. Carlin, C.K. Gelbke, W.G. Gong, Y.D. Kim, M.A. Lisa, W.G. Lynch, G.F. Peaslee, M.B. Tsang, H.M. Xu, F. Zhu, and W.A. Friedman, Phys. Lett. B **268**, 6 (1991).

[15] J. Hubele, P. Kreutz, J.C. Adloff, M. Begemann-Blaich, P. Bouissou, G. Imme, I. Iori, G.J. Kunde, S. Leray, V. Lindenstruth, Z. Liu, U. Lynen, R.J. Meijer, U. Milkau, A. Moroni, W.F.J. Müller, C. Ngô, C.A. Ogilvie, J. Pochodzalla, G. Raciti, G. Rudolf, H. Sann, A. Schüttauf, W. Seidel, L. Stuttge, W. Trautmann, and A. Tucholski, Z. Phys. A **340**, 263 (1991).

[16] C.A. Ogilvie, J.C. Adloff, M. Begemann-Blaich, P. Bouissou, J. Hubele, G. Imme, I. Iori, P. Kreutz, G.J. Kunde, S. Leray, V. Lindenstruth, Z. Liu, U. Lynen, R.J. Meijer, U. Milkau, W.F.J. Müller, C. Ngô, J. Pochodzalla, G. Raciti, G. Rudolf, H. Sann, A. Schüttauf, W. Seidel, L. Stuttge, W. Trautmann, and A. Tucholski, Phys. Rev. Lett. **67**, 1214 (1991).

[17] D.R. Bowman, G.F. Peaslee, R.T. de Souza, N. Carlin, C.K. Gelbke, W.G. Gong, Y.D. Kim, M.A. Lisa, W.G. Lynch, L. Phair, M.B. Tsang, C. Williams, N. Colonna, K. Hanold, M.A. McMahan, G.J. Wozniak, L.G. Moretto, and W.A. Friedman, Phys. Rev. Lett. **67**, 1527 (1991).

[18] G. Bizard, D. Durand, A. Genoux-Lebain, M. Louvel, R. Bougault, R. Brou, H. Doubre, Y. El-Masri, H. Fugiwara, K. Hagel, A. Hajfani, F. Hanappe, S. Jeong, G.M. Jin, S. Kato, J.L. Laville, C. le Brun, J.F. Lecolley, S. Lee, T. Matsuse, T. Motobayashi, J.P. Patry, A. Péghaire, J. Péter, N. Prot, R. Regimbart, F. Saint-Laurent, J.C. Steckmeyer, and B. Tamain, Phys. Lett. B **276**, 413 (1992).

[19] J. Hubele, P. Kreutz, V. Lindenstruth, J.C. Adloff, M. Begemann-Blaich, P. Bouissou, G. Imme, I. Iori, G.J. Kunde, S. Leray, Z. Liu, U. Lynen, R.J. Meijer, U. Milkau, A. Moroni, W.F.J. Müller, C. Ngô, C.A.

Ogilvie, J. Pochodzalla, G. Raciti, G. Rudolf, H. Sann, A. Schüttauf, W. Seidel, L. Stuttge, W. Trautmann, A. Tucholski, R. Heck, A.R. DeAngelis, D.H.E. Gross, H.R. Jaqaman, H.W. Barz, H. Schulz, W.A. Friedman, and R.J. Charity, Phys. Rev. C **46**, R1577 (1992).

[20] K. Hagel, M. Gonin, R. Wada, J.B. Natowitz, B.H. Sa, Y. Lou, M. Gui, D. Utley, G. Nebbia, D. Fabris, G. Prete, J. Ruiz, D. Drain, B. Chambon, B. Cheynis, D. Guinet, X.C. Hu, A. Demeyer, C. Pastor, A. Giorni, A. Lleres, P. Stassi, J.B. Viano, and P. Gonthier, Phys. Rev. Lett. **68**, 2141 (1992).

[21] T.C. Sangster, H.C. Britt, D.J. Fields, L.F. Hansen, R.G. Lanier, M.N. Namboodiri, B.A. Remington, M.L. Webb, M.L. Begemann-Blaich, T. Blaich, M.M. Fowler, J.B. Wilhemy, Y.D. Chan, A. Dacal, A. Harmon, J. Pouliot, R.G. Stokstad, S. Kaufman, F. Videbaek, Z. Fraenkel, G. Peilert, H. Stöcker, W. Greiner, A. Botvina, and I.N. Mishustin, Phys. Rev. C **46**, 1404 (1992).

[22] Y.D. Kim, R.T. de Souza, D.R. Bowman, N. Carlin, C.K. Gelbke, W.G. Gong, W.G. Lynch, L. Phair, M.B. Tsang, and F. Zhu, Phys. Rev. C **45**, 338 (1992);

[23] H. Stuttgé, J.C. Adloff, B. Bilwes, R. Bilwes, F. Cosmo, M. Glaser, G. Rudolf, F. Scheibling, R. Bougault, J. Colin, F. Delauney, A. Genoux-Lebain, D. Horn, C. le Brun, J.F. Lecolley, M. Louvel, J.C. Steckmeyer, and J.L. Ferrerro, Nucl. Phys. **A539**, 511 (1992).

[24] M. Colonna, P. Roussel-Chomaz, N. Colonna, M. DiToro, L.G. Moretto, and G.J. Wozniak, Phys. Lett. B **283**, 180 (1992); M. Colonna, N. Colonna, A. Bonasera, and M. DiToro, Nucl. Phys. **A541**, 295 (1992).

[25] D.R. Bowman, C.M. Mader, G.F. Peaslee, W. Bauer, N. Carlin, R.T. de Souza, C.K. Gelbke, W.G. Gong, Y.D. Kim, M.A. Lisa, W.G. Lynch, L. Phair, M.B. Tsang, C. Williams, N. Colonna, K. Hanold, M.A. McMahan, G.J. Wozniak, L.G. Moretto, and W.A. Friedman, Phys. Rev. C **46**, 1834 (1992).

[26] P. Kruetz, J.C. Adloff, M.L. Begemann-Blaich, P. Bouissou, J. Hubele, G. Immé, I. Iori, G.J. Kunde, S. Leray, V. Lindenstruth, Z. Liu, U. Lynen, R.J. Meijer, U. Milkau, A. Moroni, W.F.J. Müller, C. Ngô, C.A. Ogilvie, J. Pochodzalla, G. Raciti, G. Rudolf, H. Sann, A. Schüttauf, W. Seidel, L. Stuttge, W. Trautmann, and A. Tucholski, Nucl. Phys. **A556**, 672 (1993).

[27] M.B. Tsang, W.C. Hsi, W.G. Lynch, D.R. Bowman, C.K. Gelbke, M.A. Lisa, G.F. Peaslee, G.J. Kunde, M.L. Begemann-Blaich, T. Hofmann, J. Hubele, J. Kempter, P. Kreutz, W.D. Kunze, V. Lindenstruth, U. Lynen, M. Mang, W.F.J. Müller, M. Neumann, B. Ocker, C.A. Ogilvie, J. Pochodzalla, F. Rosenberger, H. Sann, A. Schüttauf, V. Serfling, J. Stroth, W. Trautmann, A. Tucholski, A. Wörner, E. Zude, B. Zwieglinski, S. Aiello, G. Immé, V. Pappalardo, G. Raciti, R.J. Charity, L.G. Sobotka, I. Iori, A. Moroni, R. Scardoni, A. Ferrero, W. Seidel, Th. Blaich, L. Stuttge, A. Cosmo, W.A. Friedman, and G. Peilert, Phys. Rev. Lett. **71**, 1502 (1993).

[28] G.D. Westfall, J.E. Yurkon, J. Van Der Plicht, Z.M. Koenig, B.V. Jacak, R. Fox, G.M. Crawley, M.R. Maier, B.E. Hasselquist, R.S. Tickle, and D. Horn, Nucl. Instrum. Methods Phys. Res. Sect. A **238**, 347 (1985).

[29] G.D. Westfall, W. Bauer, D. Craig, M. Cronqvist, E. Gualtieri, S. Hannuschke, D. Klakow, T. Li, T. Reposeur, A.M. Vander Molen, W.K. Wilson, J.S. Winfield, J. Yee, S.J. Yennello, R.A. Lacey, A. Elmaani, J. Lauret, A. Nadasen, and E. Norbeck, Phys. Rev. Lett. **71**, 1986

(1993); E. Bauge, A. Elmaani, R.A. Lacey, J. Lauret, N.N. Ajitanand, D. Craig, M. Cronqvist, E. Gualtieri, S. Hannuschke, T. Li, W.J. Llope, T. Reposeur, A.M. Vander Molen, G.D. Westfall, J.S. Winfield, J. Yee, S.J. Yennello, A. Nadasen, and E. Norbeck, *ibid.* **70**, 3705 (1993); T. Li, W. Bauer, D. Craig, M. Cronqvist, E. Gualtieri, S. Hannuschke, R.A. Lacey, W.J. Llope, T. Reposeur, A.M. Vander Molen, G.D. Westfall, W.K. Wilson, J.S. Winfield, J. Yee, S.J. Yennello, A. Nadasen, R.S. Tickle, and E. Norbeck, *ibid.* **70**, 1924 (1993); R.A. Lacey, A. Elmaani, J. Lauret, T. Li, W. Bauer, D. Craig, M. Cronqvist, E. Gualtieri, S. Hannuschke, T. Reposeur, A.M. Vander Molen, G.D. Westfall, W.K. Wilson, J.S. Winfield, J. Yee, S.J. Yennello, A. Nadasen, R.S. Tickle, and E. Norbeck, *ibid.* **70**, 1224 (1993).

[30] L. Phair, D.R. Bowman, C.K. Gelbke, W.G. Gong, Y.D. Kim, M.A. Lisa, W.G. Lynch, G.F. Peaslee, R.T. de Souza, M.B. Tsang, and F. Zhu, Nucl. Phys. **A548**, 489 (1992).

[31] G. Fái and J. Randrup, Nucl. Phys. **A404**, 551 (1983).

[32] C. Cavata, M. Demoulins, J. Gosset, M.C. Lemaire, D. L'Hôte, J. Poitou, and O. Valette, Phys. Rev. C **24**, 1760 (1990).

[33] D.H.E. Gross, Prog. Part. Nucl. Phys. **30**, 155 (1993), and references therein.

[34] J.P. Bondorf, R. Donangelo, I.N. Mushistin, C.J. Pethick, H. Schulz, and K. Sneppen, Nucl. Phys. **A443**, 321 (1985); J.P. Bondorf, R. Donangelo, I.N. Mushistin, and H. Schulz, *ibid.* **A444**, 460 (1985).

[35] R.J. Charity, M.A. McMahan, G.J. Wozniak, R.J. McDonald, L.G Moretto, D.G. Sarantites, L.G. Sobotka, G. Guarino, A. Pantaleo, L. Fiore, A. Gobbi, and K.D. Hildenbrand, Nucl. Phys. **A483**, 371 (1988).

[36] W. Bauer, G.F. Bertsch, W. Cassing, and U. Mosel, Phys. Rev. C **34**, 2127 (1986); W. Bauer, Phys. Rev. Lett. **61**, 2534 (1988).

[37] C.M. Mader, Ph.D. thesis, Michigan State University, 1993 (unpublished).

[38] K. Kwiatkowski, W.A. Friedman, L.W. Woo, V.E. Viola, E.C. Pollacco, C. Volant, and S.J. Yennello, Phys. Rev. C **49**, 1516 (1994).

[39] J. Aichelin and H. Stöcker, Phys. Lett. B **176**, 14 (1986); J. Aichelin, G. Peilert, A. Bohnet, A. Rosenhauer, H. Stöcker, and W. Greiner, Phys. Rev. C **37**, 2451 (1988); G. Peilert, J. Konopka, H. Stöcker, W. Greiner, M. Blann, and M.G. Mustafa, *ibid.* **46**, 1457 (1992).

[40] W.A. Friedman and W.G. Lynch, Phys. Rev. C **28**, 16 (1983); **28**, 950 (1983).

[41] H. Stöcker, G. Buchwald, G. Graebner, P. Subramanian, J.A. Maruhn, W. Greiner, B.V. Jacak, and G.D. Westfall, Nucl. Phys. **A400**, 63c (1983); D. Hahn and H. Stöcker, *ibid.* **A476**, 718 (1988); Phys. Rev. C **37**, 1048 (1988).

[42] W.A. Friedman (private communication).

[43] W.A. Friedman, Phys. Rev. C **42**, 667 (1990).

[44] D.H. Boal and J.N. Glosli, Phys. Rev. C **37**, 91 (1988); **42**, R502 (1990).

[45] R. Donangelo, H. Schulz, K. Sneppen, and S.R. Souza, Phys. Rev. C **50**, R563 (1994).